5-2015

Simulations of nanoscale Ni/Al multilayer foils with intermediate Ni2Al3 growth

I. E. Gunduz
Purdue University

S. Onel
Hacettepe University

C. C. Doumanidis
Khalifa University

C. Rebholz
University of Cyprus

Steven F. Son
Purdue University, sson@purdue.edu

Recommended Citation

I. E. Gunduz, S. Onel, C. C. Doumanidis, C. Rebholz, and S. F. Son, "Simulations of nanoscale Ni/Al multilayer foils with intermediate Ni2Al3 growth," Journal of Applied Physics, 117(21), 214904 (2015), http://dx.doi.org/10.1063/1.4921906.

Simulations of nanoscale Ni/Al multilayer foils with intermediate Ni_2Al_3 growth

I. E. Gunduz, S. Onel, C. C. Doumanidis, C. Rebholz, and S. F. Son

Citation: Journal of Applied Physics **117**, 214904 (2015);
View online: https://doi.org/10.1063/1.4921906
View Table of Contents: http://aip.scitation.org/toc/jap/117/21
Published by the American Institute of Physics

Simulations of nanoscale Ni/Al multilayer foils with intermediate Ni_2Al_3 growth

I. E. Gunduz,[1,a)] S. Onel,[2] C. C. Doumanidis,[3] C. Rebholz,[4] and S. F. Son[1]
[1]*School of Mechanical Engineering, Purdue University, West Lafayette, Indiana 47907, USA*
[2]*Department of Chemical Engineering, Hacettepe University, Ankara 06800, Turkey*
[3]*Department of Mechanical Engineering, Khalifa University, Abu Dhabi, United Arab Emirates*
[4]*Mechanical and Manufacturing Engineering Department, University of Cyprus, 1678 Nicosia, Cyprus*

(Received 24 March 2015; accepted 20 May 2015; published online 4 June 2015)

Nanoscale multilayers of binary metallic systems, such as nickel/aluminum, exhibit self-propagating exothermic reactions due to the high formation enthalpy of the intermetallic compounds. Most of the previous modeling approaches on the reactions of this system rely on the use of mass diffusion with a phenomenological derived diffusion coefficient representing single-phase (NiAl) growth, coupled with heat transport. We show that the reaction kinetics, temperatures, and thermal front width can be reproduced more satisfactorily with the sequential growth of Ni_2Al_3 followed by NiAl, utilizing independently obtained interdiffusivities. The computational domain was meshed with a dynamically generated bi-modal grid consisting of fine and coarse zones corresponding to rapid and slower reacting regions to improve computational efficiency. The PDEPE function in MATLAB was used as a basis for an alternating direction scheme. A modified parabolic growth law was employed to model intermetallic growth in the thickness direction. A multiphase enthalpy function was formulated to solve for temperatures after discrete phase growth and transformations at each time step. The results show that the Ni_2Al_3 formation yields a preheating zone to facilitate the slower growth of NiAl. At bilayer thicknesses lower than 12 nm, the intermixing layer induces oscillating thermal fronts, sharply reducing the average velocities. © *2015 AIP Publishing LLC*.
[http://dx.doi.org/10.1063/1.4921906]

I. INTRODUCTION

Self-propagating exothermic reactions (SPER) in multilayer films/foils (MF) of reactive metallic systems such as nickel (Ni) and aluminum (Al) have been increasingly studied since the earlier work by Munir *et al.*[1] Such reactive systems can be used for joining temperature-sensitive components due to the localized nature of heat generation, or for bulk synthesis and near-net *in-situ* forming of intermetallic parts.[2–12] Although the MFs of the Ni-Al system have been characterized by increasingly sophisticated characterization methods such as dynamic transmission electron microscopy (DTEM)[13–15] and X-Ray diffraction (XRD) using synchrotron radiation,[16–19] the exact nature of the reactions has remained elusive. This is due to the limitations of these methods to resolve details of a reactive propagating at high reaction speeds that can reach 13 m/s at individual bilayer thicknesses on the order of 20 nm for the Ni-Al system and correspondingly thin reaction zones.[20] This complicates modeling efforts, the accuracy of which depends heavily on the proposed reaction mechanism and phase formation sequence.

Differential scanning calorimetry (DSC) studies of the nanoscale Ni-Al multilayers show that phases form incrementally at temperatures as low as ~500 K starting with Ni_2Al_9 or $NiAl_3$, followed by more Ni-rich phases such as Ni_2Al_3 or NiAl depending on the overall composition and the bilayer thickness.[21,22] This behavior is different from the results of experiments performed by immersing solid Ni rods in liquid Al, which show that the major phase that forms is Ni_2Al_3 at temperatures up to 1190 K, accompanied by the formation of $NiAl_3$ in small amounts.[23,24] Interestingly, the NiAl phase is not observed, which forms at much lower temperatures during DSC analysis of MFs. Additionally, the phase formation sequence observed during DSC is consistent with slow reacting geometries such as powder mixtures or coarse multilayers with lower reaction rates. In these cases, *in-situ* XRD results[25] or thermal analysis[9] verify a sequential formation of phases $NiAl_3$, Ni_2Al_3, and NiAl, although the temperatures are much higher, more closely following equilibrium limits in the Ni-Al phase diagram.[9] Nanocalorimeter experiments performed in a DTEM system up to heating rates of $\sim 10^3$ K/s showed a phase formation sequence similar to DSC analysis with lower heating rates.[26] *In-situ* analysis methods on reacting MFs with DTEM[12–14] or XRD with synchrotron radiation still lack the required angular[17] and/or temporal resolution[16,18] required to distinguish the phases that form during SPER of nanoscale MFs, which have self-heating rates on the order of 10^6 K/s. The Ni-Al system is especially difficult to characterize as most of the phases have overlapping diffraction peaks that make accurate identification challenging. Rapid quenching is another approach, where results with foils with front velocities around 9.5 m/s show the formation of multiple zones within a width of approximately 10–30 μm, which are attributed to solid and liquid diffusion and nucleation of NiAl grains within the

[a)]Author to whom correspondence should be addressed. Email: igunduz@purdue.edu. Tel.: (765) 494-0066. Fax: (765) 494-0530.

melt.[27,28] This result is not compatible with an overall process governed by a single diffusivity value, where the maximum reaction width can be estimated to be much sharper about $\sim 3\ \mu$m at the same conditions.

There is extensive literature aimed at modeling the reactions in the Ni-Al system starting with early simple analytical methods applied to MFs[10,29] to more sophisticated computational methods taking into account melting or variable thermal diffusivity[30,31] in 1D to 3D geometries.[32] All of these studies consider heat generation from mixing/reaction in a continuous diffusive field characterized with a single[4,32] or multiple[33] ad-hoc diffusivity values coupled with a thermal field to match the velocity measurements. Although this phenomenological approach is powerful for estimating velocities, it cannot describe accurate transient microstructures. Most of these computational studies employ the adiabatic reaction assumption and symmetric boundary conditions applied to a single bilayer, where the heat losses due to conduction within a substrate, convection, and radiation heat transfer and variations in temperature along the thickness of the foils are ignored. More recent studies used reduced models to simulate substrate heating or 2D thermal wave kinetics within reasonable computational times.[32,33] In contrast, our previous work proposed a different approach employing a two-step reaction with the sequential 1D growth of Ni_2Al_3 and NiAl laterally using independently measured interdiffusivity values,[30] which can successfully predict the experimentally measured reaction velocities and better reflect the observed phase formation observed in solid Ni and liquid Al experiments.[1,23,24] The model however was limited to a single bilayer and suffered from numerical instabilities due to Crank-Nicolson method.

This paper employs an extension of Ref. 30, assuming a similar two-step reaction scheme with the sequential formation of Ni_2Al_3 and NiAl over a dynamic bi-modal grid, aiming to not only obtain thermal profiles but also *in-situ* microstructural evolution within a multiple layer foil during the reaction. Furthermore, a nodal enthalpy polynomial was formulated to enable the incorporation of the growth and transformation of multiple discrete phases into the continuous thermal field. For the numerical solver, a robust MATLAB module (PDEPE) was used sequentially in multiple dimensions to minimize numerical errors and spurious oscillations.

II. NUMERICAL MODEL

The numerical model is based on the following assumptions: (1) the intermetallic growth takes place only in the thickness (lateral) direction (1D) within a grid element (mass diffusion between adjacent grid points is ignored), is diffusion limited, and obeys a parabolic growth law for Ni_2Al_3 and NiAl; (2) the intermixing at the interfaces due to co-sputtering can be modeled as an equivalent layer of Ni_2Al_3 to simplify the analysis; (3) the dissolution of Ni in liquid Al is ignored; and (4) the intermetallic phases and the liquid NiAl are assumed to be stoichiometric. The seven phases that are considered in the model are solid and liquid Al, solid and liquid Ni, solid and liquid NiAl, and solid Ni_2Al_3. The phase fractions for all nodes, which consist of a half-bilayer at a single temperature, are stored in matrices at each time step (Figure 1). The computational grid consists of a fine zone where the fast reactions and primary thermal diffusion occurs, which is surrounded by a coarser grid where the temperature transients are lower.

Fine grid sizes in the in-plane directions were varied depending on the bilayer thickness from 250 nm to 4000 nm for bilayer thicknesses of 10 nm and 160 nm, respectively, with time steps between 0.5 ns and 10 ns. The spatial and temporal steps were chosen to minimize temperature overshooting due to rapid intermetallic growth at the maximum front temperature and oscillations, as described in Ref. 30. The remaining areas are modeled using a coarser mesh on each side of the thermal front, and additional 10 grid points with the fine grid size were introduced between the fine and coarse grids to minimize numerical errors at the transition points. The limits of the fine zone are taken as the first occurrence of the adiabatic temperature behind the thermal front and 1 K above initial temperature ahead of the front. In the thickness direction (z), the half-bilayer thickness is the naturally arising grid size. Since this is usually much less than the longitudinal grid size (x), a certain number of half-bilayers corresponding to the thickness grid sizes are lumped in a grid point to match the x grid size. For example, for a half-bilayer thickness of 20 nm and an x grid size of 1000 nm, it was assumed that 50 half-bilayers have identical phase percentages and temperatures, so that the grid size in z direction is also 1000 nm. For thinner foils, a lower number of half-bilayers was used (2 for 125 nm foil thickness).

The volumetric nodal enthalpies H_t^{node} can be expressed as a function of temperature and phase fractions

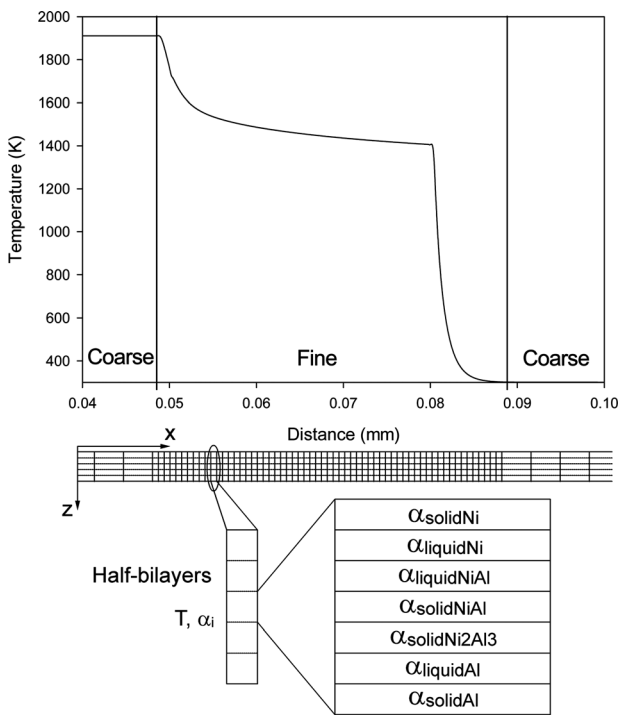

FIG. 1. A typical stable thermal profile (bilayer = 40 nm) demonstrating the domain boundaries for fine and coarse grid zones in the x-direction (in plane), along with the lumped bilayer nodes consisting of different phases.

$$H_t^{node} = \frac{1}{T}\left(\sum_{i=1}^{7}\alpha^i A^i\right) + \left(\sum_{i=1}^{7}\alpha^i B^i\right) + T\left(\sum_{i=1}^{7}\alpha^i C^i\right) + T^2\left(\sum_{i=1}^{7}\alpha^i D^i\right) + T^3\left(\sum_{i=1}^{7}\alpha^i E^i\right) \quad (1)$$

where T is the temperature, α^i is the volume fraction of phase i, and A^i to E^i are the coefficients of the integral of the volumetric specific heat polynomial for phase i (Table I). This expression and its temperature derivative can be used to calculate the nodal specific heat and enthalpy, given the temperature and phase fractions. Conversely, given phase fractions and nodal enthalpy, the temperature can be calculated from the roots of this 4th order polynomial as well. The correct root is easily selected as the other three roots are either complex or below the initial temperature of 300 K in all cases. This is used for updating temperatures when the phase fractions change due to intermetallic growth at constant enthalpy within the time step.

For each node, the intermetallic thicknesses X^{int} as a function of time t can be expressed using the parabolic growth law

$$X^{\text{int}} = \sqrt{\frac{2\gamma D^{\text{int}} t}{\beta}}, \quad (2)$$

where D^{int} is the interdiffusivity of the intermetallic that has an Arrhenius form $D^{\text{int}} = D_0 \cdot \exp\left(-\frac{Q}{R\cdot T}\right)$, γ is a constant for modifying the growth rates within experimental uncertainties (where 1 is the nominal value), and β is a growth factor derived from mass conservation given by

$$\beta = \frac{(N^{\text{int}} - N^{Al})(N^{Ni} - N^{\text{int}})}{(N^{Ni} - N^{Al})}, \quad (3)$$

where N^{int}, N^{Al}, and N^{Ni} are the mole percents of the intermetallic, the Al-rich side, and the Ni-rich side of the intermetallic, respectively.[34] The Ni-Al phase diagram shows that Al-rich solid phase has almost no Ni solubility and the composition is always close to 0 at. % Ni. The Ni-rich phase has some Al solubility and can have compositions within the range of 80–90 at. % Ni depending on the temperature. For an average value of 85 at. % Ni, β is approximately 0.2 for the two intermetallics NiAl and Ni_2Al_3. Equation (2) in this form cannot be directly used as the temperature changes during the intermetallic growth. By rearranging the terms, an equivalent time t_{eq} can be calculated using

$$t_{eq} = \frac{\beta}{2\gamma D^{\text{int}}(T_t)} \cdot \left(X_t^{\text{int}}\right)^2, \quad (4)$$

which is the time it would take for the intermetallic to grow to the current thickness X_t^{int} at the current temperature T_t. The amount of growth dX_t^{int} arising at this initial state (t_{eq}, X_t^{int}, T_t) after the time step Δt can be calculated by

$$dX_t^{\text{int}} = \sqrt{\frac{2\gamma D^{\text{int}}(T_t)\cdot(t_{eq}+\Delta t)}{\beta}} - X_t^{\text{int}}. \quad (5)$$

For the interdiffusivities, we used the reported value for Ni_2Al_3[35] and NiAl at a composition of Ni(0.47)-Al(0.53), the overall composition in sputtered foils without vanadium (V).[36] Values of 0.4 and 2 for γ were used for Ni_2Al_3 and NiAl, respectively. It was assumed that the fastest growing phase at a given temperature grows first, which was Ni_2Al_3 at all temperatures. For the effects of intermixing layer that forms during sputtering, an initial Ni_2Al_3 layer with a thickness of 2.35 nm was used for all bilayer thicknesses, based on the amount of heat output during DSC,[20] which produced the best match to the velocity curve. The thermodynamic and physical properties used are shown in Table I.

The numerical solution was performed using the PDEPE nonlinear PDE solver function in MATLAB over the bimodal grid. PDEPE solves initial-boundary value problems for systems of parabolic and elliptic PDEs in the one space variable x and time t. The solver converts the PDEs to ODEs using a second-order accurate spatial discretization based on a fixed set of user-specified nodes in a manner described in Ref. 37. The time integration is done with the stiff ODE solver ODE15S, which adjusts the time step dynamically within the time range given. PDEPE was employed sequentially for each coordinate to use it as an alternating direction scheme. Since the rapid heat generation due to intermetallic growth limits the time steps to a few ns, this does not introduce significant errors in the temperature field. The solver was used to solve the temperature profile for a single time step (0.5–10 ns), where the previous solution step was used as the initial condition for the next step. This enables incorporation of non-linear heat generation through the use of the parabolic growth and phase transformation results that were used to directly calculate the temperatures while avoiding iterative methods. After the new temperatures are calculated,

TABLE I. Enthalpies (J/mole), molar volumes, prediffusion factor, and activation energy (kJ/mole) of interdiffusivity of the phases considered.[9,35,36,38–40]

		A × 10^{-5}	B × 10^{-3}	C	D × 10^{3}	E × 10^{6}	Molar volume (cm^3/mole)	Interdiffusivity (D_0, Q)
Solid Al[38]		3.6	−10.014	31.38	−8.2	6.91667	9.993	
Liquid Al[38]		0	−0.795	31.75	0	0	11.31	
Solid Ni[38]	T < = 631	−3.18	−3.939	11.17	18.89	0	6.594	
	T > 631	−15.4	−2.4	20.54	5.04	0		
Liquid Ni[38]		0	−9.549	43.1	0	0	7.424	
Solid Ni_2Al_3[39]		0	−315.5	106.06	17.155	0	41.66[9]	9.772×10^{-3}, 199[35]
Solid NiAl[38]		0	−131.489	41.84	6.905	0	14.16	4.54×10^{-5}, 235[36]
Liquid NiAl[38]		0	−111.75	74.85	0	0	16.65	1.404×10^{-6}, 51.48[40]

the new transition temperature locations are determined to update the grid if necessary. All the nodal specific quantities such as temperature and phase fractions are evaluated at the new node positions using the PDEVAL interpolating function in MATLAB. The solution steps are shown in Figure 2, where T and α represent the temperature and phase fractions at the current time step for each node, respectively.

Since the phase transformations and the corresponding temperature changes are explicitly determined, the heat equation with no source term is used for time stepping the temperature

$$\rho C_p \frac{\partial T}{\partial t} = k \cdot \nabla^2 T, \tag{6}$$

where ρ is the density, C_p is the specific heat, and k is the thermal conductivity with a volume averaged value of 150 W/mK. The product ρC_p was evaluated from the derivative of the enthalpy polynomial, so it is a volume average of all the phases at each node at a given temperature. Instead of using a source term, local temperatures at each time step are obtained from intermetallic growth or phase transformations using Eqs. (1)–(5). The resulting temperatures and updated nodal properties (ρ, C_p) are used as the initial condition to evolve the temperature field in the next time step. Convective and radiative boundary conditions were also imposed to include heat loss effects. The ignition was initiated by holding one boundary at the calculated adiabatic temperature for a limited duration until the front became self-propagating.

III. RESULTS

A. Velocity dependence on bilayer thickness

The velocity of the flame front as a function of bilayer thickness is given in Fig. 3, along with experimentally

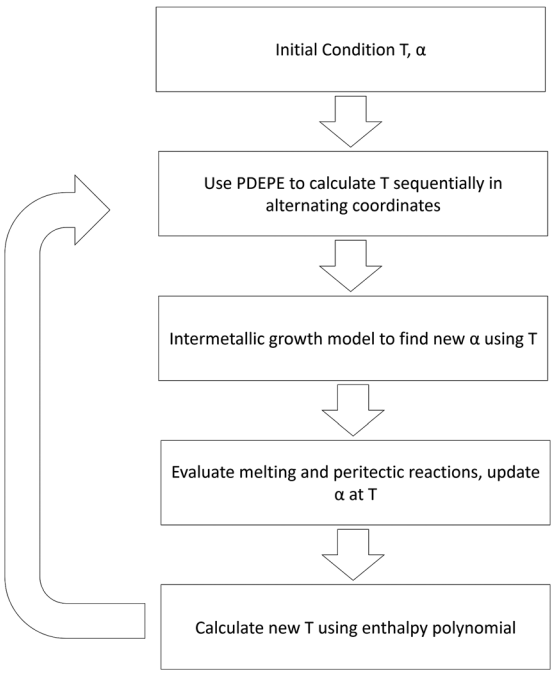

FIG. 2. The numerical solution steps where T and α represent the temperature and phase fractions at the current time step for each node, respectively.

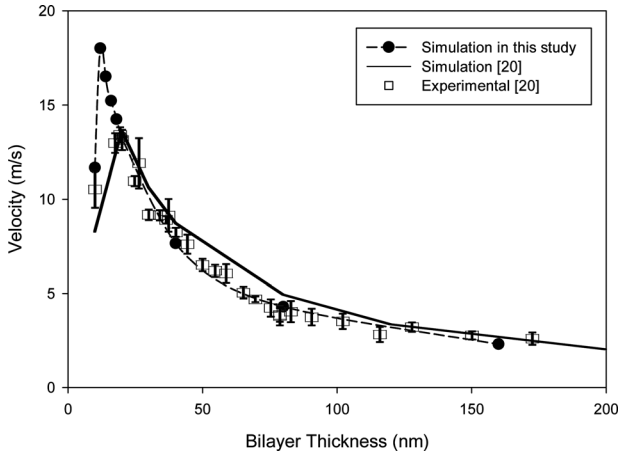

FIG. 3. Computational results for velocity variation with bilayer thickness along with experimental measurements and previous simulations.[20]

measured values and other modeling results.[20] The calculated values follow the measured values closely, reproducing both small and very large bilayer trends. The agreement is more precise than Ref. 20 but very comparable to more recent results in Ref. 33 that uses three different diffusion coefficients. The intermixed layer arising from co-sputtering starts dominating the kinetics below a bilayer thickness of 12 nm, where the average velocity abruptly decreases due to the onset of oscillations of the reaction front. This results from a reduction in the amount of available energy and the subsequent drop in the adiabatic temperature. This type of behavior is different from analytical solutions, which produce a more gradual transition in velocity at lower bilayer thicknesses. The analysis here was performed in 2 nm steps in the bilayer range of 10–20 nm and predicts a rather large velocity spike before oscillations set in. Unfortunately, there is no experimental data for this bilayer range except at 10 nm and 20 nm, so a direct comparison with experiments or other numerical studies was not possible. For the larger bilayer thicknesses, the effect of intermixed zone becomes negligible, where an expected inverse proportionality with velocity based on diffusion limited growth is observed.

B. Thermal fronts and corresponding microstructures

A typical steady-state thermal profile is shown in Fig. 4 for a bilayer thickness of 20 nm. The profiles are characterized by a heated zone ahead of the front (Zone 1), a rapid temperature rise zone dominated by Ni_2Al_3 growth (Zone 2), a gradual temperature rise zone due to the slower growth rate of NiAl (Zone 3), and a fully reacted area (Zone 4). After the initial ignition stage, Zone 3 width reduces or increases depending on the way ignition is imposed and eventually reaches a unique steady-state value. This is due to the varying thermal gradient and the heat fluxes between Zones 2–3 and Zones 3–4. The width of the areas where there is a phase change such as Al and Ni melting and peritectic decomposition of Ni_2Al_3 are very narrow and confined to a few μm, indicating that the reaction releases enough heat to allow these endothermic transformations to progress rapidly. In general, the widths of all the zones increase with increasing

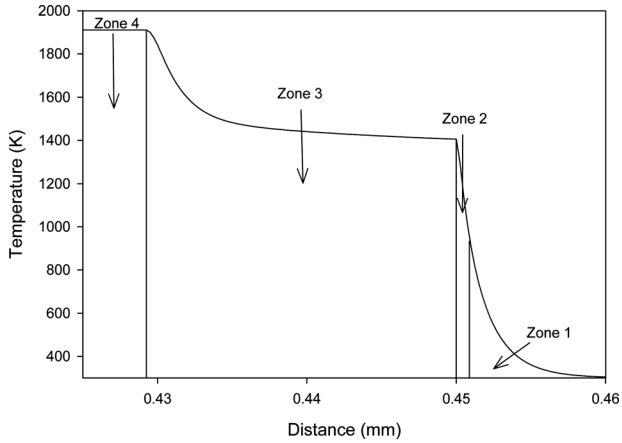

FIG. 4. Thermal profile for a bilayer thickness of 20 nm, showing the different reaction zones within the front.

bilayer thickness, as the slower kinetics allow heat to diffuse further from the reaction front, as shown in Fig. 5.

For an oscillating case with a bilayer thickness of 10 nm, the evolution of the thermal profile is shown in Fig. 6, where the adiabatic temperature is ~1638 K. The front evolves with super-adiabatic excursions followed by cool zones. Boundary 2 initially moves at a high velocity, expected from the inverse proportionality to the bilayer thickness. Boundary 3 is not able to sustain this velocity because of the lower adiabatic temperatures (compared to 1911 K) and NiAl growth rates, causing Zone 3 to widen. At some point, this stalls the motion of Boundary 2 because of the reduction in the thermal gradient, causing a widening of Zone 2 with more thermal diffusion. The growth of Ni_2Al_3 within this zone continues but NiAl does not form because the temperature remains below 1406 K. As Boundary 3 approaches the stalled Boundary 2, the heat flow into Zone 2 is increased. This, coupled with the growth of Ni_2Al_3 within a wider area, results in overshooting of the local temperatures above the adiabatic value, reaching ~1800 K, while at the same time leaving behind a low temperature area around ~1300 K. This recovers the high velocity of the Boundary 2, and the process is repeated. This oscillating motion leaves a

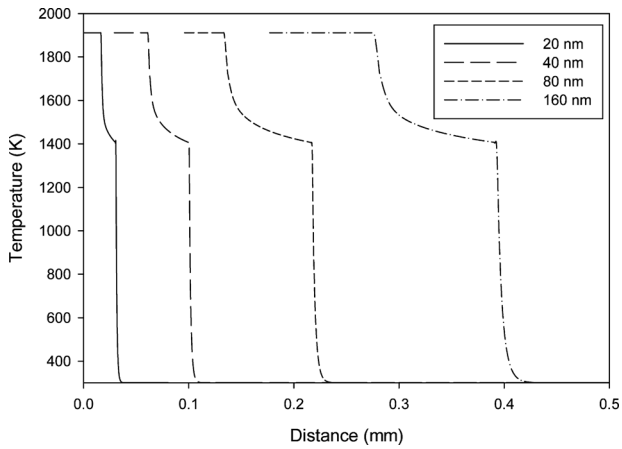

FIG. 5. Stable thermal profiles for different bilayer thicknesses. The width of the reaction zone scales linearly with bilayer thickness until the intermixing effects start to dominate at around 20 nm.

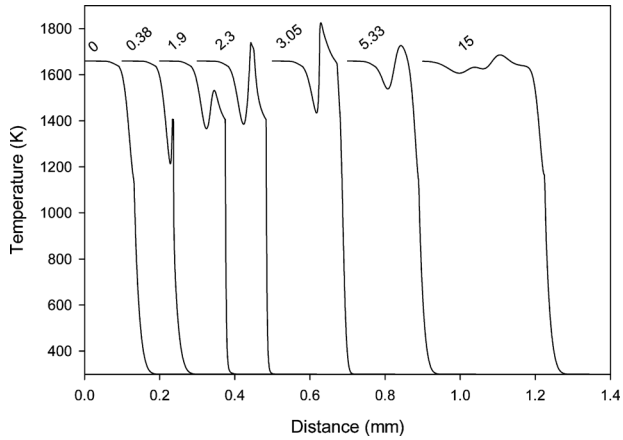

FIG. 6. Transient thermal profiles for the oscillating reactions at 10 nm bilayer thickness. Each curve is marked with its relative time in microseconds.

wake of thermal waves, which eventually reach a uniform temperature of ~1638 K, i.e., the adiabatic temperature.

The corresponding phase percentages also vary with bilayer thickness as demonstrated in Fig. 7 for the bilayer thickness of 20 nm. As the bilayer thickness increases, the effect of intermixing, which represents an overall enthalpy loss, diminishes and the percentage of molten NiAl increases after the reaction, reaching the adiabatic limits. Even after the temperature reaches 1911 K, the growth of NiAl continues since there are still reactants left, which results in further NiAl melting. The resulting transient structure can be expected to be a mixture of nanoscale solid NiAl particles surrounded by liquid NiAl. Further numerical evolution of the microstructures during the cooling stage has not been investigated, as it includes different mechanisms like recrystallization and grain growth.

Analysis of foils with an overall thickness of 125 nm and bilayer thicknesses of 21 nm using an intermixing zone width of 1 nm, resulted in a velocity of 13 m/s, which compares favorably with the experimental results on the *in-situ* morphology of the reaction front observed using DTEM for different overall compositions (Ni:Al molar ratios of 3:2, 1:1, and 2:3).[13–15] In Ref. 13–15, three characteristic areas

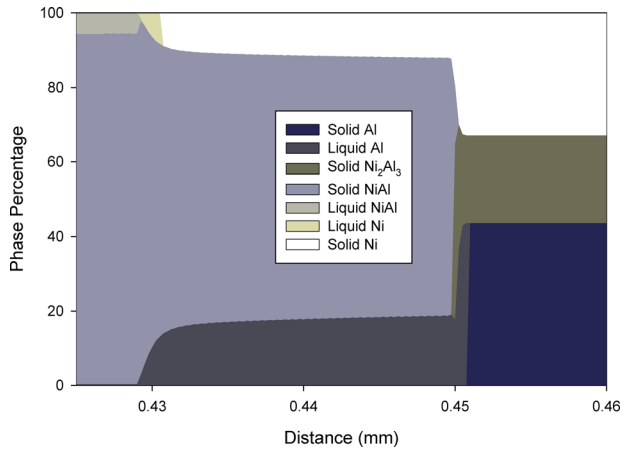

FIG. 7. Stable phase percentages of a single bilayer for a bilayer thickness of 20 nm.

were distinguishable: the area ahead of the reaction front where the original structure remained, an intermediate zone consisting of NiAl with possibly some of the original reactants showing cellular morphology, followed by a fully reacted area. It was noted that some of these structures remained after cooling around certain areas of the foils.[13] The reported formation of the intermediate zone had a dependence on overall composition; it was absent at the stoichiometric NiAl composition, but extended up to 40 μm at Ni-rich compositions. The results from the simulations are qualitatively similar to Figures 3, 4, and 6 and show that the width of the area where Ni_2Al_3 forms and grows is very small (around 2 μm) and lasts for ~150 ns, which cannot be resolved experimentally.[13–15] The total width of the area where NiAl grew from liquid Al and solid/liquid Ni until the reaction was complete was about 20 μm. This value is compatible with the reaction width in quenching experiments (~30 μm for 9.5 m/s).[27,28] The observation of the cellular morphology is possibly due to the remaining liquid that incorporates into the NiAl phase,[14] but the model in its current form cannot capture this behavior and has to be modified to allow such transitions. The heat losses for these foils were negligible, which reacted near adiabatically reaching ~1911 K. This is in agreement with *in-situ* XRD results with a very high angular resolution showing similar temperatures for thicker foils (~55 μm) with a bilayer thickness of ~50 nm,[16] where the temperature remained steady for a relatively long time (~20 ms),[16] indicating a two-phase mixture of solid and liquid NiAl.

IV. CONCLUSIONS

The model developed successfully captures the experimental velocity versus bilayer trends and thermal front properties for nanoscale Ni-Al foils using diffusion data of the intermetallics Ni_2Al_3 and NiAl. The results show that the rapid formation of Ni_2Al_3 within a few μm zone generates enough heat to drive the growth of NiAl and to support the thermal front velocities. The thermal front widths, where the conversion of constituents to NiAl was complete, were estimated to be between 20 and 120 μm for bilayer thicknesses of 20–160 nm. In contrast to analytical solutions that predict gradual decreases in velocity at low bilayer thicknesses (<20 nm) due to intermixing, the numerical results show an abrupt transition marked by the onset of oscillations. The model can be used for simulations of large geometries to determine transient thermal and phase fields, or for simulating other reactive systems that have diffusion limited kinetics.

ACKNOWLEDGMENTS

This work was supported by the European Commission under Marie Curie Excellence Team—NanoHeaters (EXT-0023899) and Marie Curie Chair—UltraNanoMan (EXC-006680), and by the Department of Energy, National Nuclear Security Administration under Award Number DENA0002377, and Defense Threat Reduction Agency (DTRA) Grant Number HDTRA1-10-1-0119.

[1]Z. A. Munir and U. Anselmi-Tamburini, Mater. Sci. Rep. **3**(7–8), 277 (1989).
[2]A. B. Mann, A. J. Gavens, M. E. Reiss, D. V. Heerden, G. Bao, and T. P. Weihs, J. Appl. Phys. **82**(3), 1178 (1997).
[3]E. Besnoin, S. Cerutti, O. M. Knio, and T. P. Weihs, J. Appl. Phys. **92**(9), 5474 (2002).
[4]A. J. Gavens, D. V. Heerden, A. B. Mann, M. E. Reiss, and T. P. Weihs, J. Appl. Phys. **87**(3), 1255 (2000).
[5]A. J. Swiston, Jr., T. C. Hufnagel, and T. P. Weihs, Scr. Mater. **48**, 1575 (2003).
[6]J. Wang, E. Besnoin, A. Duckham, S. J. Spey, M. E. Reiss, O. M. Knio, M. Powers, M. Whitener, and T. P. Weihs, Appl. Phys. Lett. **83**(19), 3987 (2003).
[7]P. Zhu, J. C. M. Li, and C. T. Liu, Mater. Sci. Eng. A **239–240**, 532 (1997).
[8]H. P. Li and J. A. Sekhar, J. Mater. Sci. **30**, 4628 (1995).
[9]P. Zhu, J. C. M. Li, and C. T. Liu, Mater. Sci. Eng. A **329–331**, 57 (2002).
[10]T. S. Dyer, Z. A. Munir, and V. Ruth, Scr. Metall. Mater. **30**(10), 1281 (1994).
[11]K. Morsi, Mater. Sci. Eng. A **299**, 1 (2001).
[12]C. Rebholz, I. E. Gunduz, T. Ando, and C. C. Doumanidis, Mater. Res. Exp. **2**, 045009 (2015).
[13]J. S. Kim, T. LaGrange, B. W. Reed, M. L. Taheri, M. R. Armstrong, W. E. King, N. D. Browning, and G. H. Campbell, Science **321**, 1472 (2008).
[14]J. S. Kim, T. LaGrange, B. W. Reed, R. Knepper, T. P. Weihs, N. D. Browning, and G. H. Campbell, Acta Mater. **59**(9), 3571 (2011).
[15]T. LaGrange, G. H. Campbell, B. W. Reed, M. L. Taheri, J. B. Pesavento, J. S. Kim, and N. D. Browning, Ultramicroscopy **108**, 1441 (2008).
[16]K. Fadenberger, I. E. Gunduz, C. Tsotsos, M. Kokonou, S. Gravani, S. Brandstetter, A. Bergamaschi, B. Schmitt, P. H. Mayrhofer, C. C. Doumanidis, and C. Rebholz, Appl. Phys. Lett. **97**, 144101 (2010).
[17]J. C. Trenkle, L. J. Koerner, M. W. Tate, S. M. Gruner, T. P. Weihs, and T. C. Hufnagel, Appl. Phys. Lett. **93**, 081903 (2008).
[18]C. S. Yoo, H. Wei, J. Y. Chen, G. Shen, and P. Chow, Rev. Sci. Instrum. **82**, 113901 (2011).
[19]J. C. Trenkle, L. J. Koerner, M. W. Tate, N. Walker, S. M. Gruner, T. P. Weihs, and T. C. Hufnagel, J. Appl. Phys. **107**, 113511 (2010).
[20]R. Knepper, M. R. Snyder, G. Fritz, K. Fisher, and O. M. Knio, J. Appl. Phys. **105**, 083504 (2009).
[21]K. J. Blobaum, D. V. Heerden, A. J. Gavens, and T. P. Weihs, Acta Mater. **51**, 3871 (2003).
[22]C. Michaelsen, G. Lucadamo, and K. Barmak, J. Appl. Phys. **80**(12), 6689 (1996).
[23]J. F. Zhao, C. Unuvar, U. Anselmi-Tamburini, and Z. A. Munir, Acta Mater. **55**, 5592 (2007).
[24]J. F. Zhao, C. Unuvar, U. Anselmi-Tamburini, and Z. A. Munir, Acta Mater. **56**, 1840 (2008).
[25]D. Tingaud, L. Stuppfler, S. Paris, D. Vrel, F. Bernard, C. Penot, and F. Nardou, Int. J. Self-Propag. High-Temp. Synth. **16**(1), 12 (2007).
[26]M. D. Grapes, T. LaGrange, K. Woll, B. W. Reed, G. H. Campbell, D. A. LaVan, and T. P. Weihs, APL Mater. **2**, 116102 (2014).
[27]A. S. Rogachev, S. G. Vadchenko, and A. S. Mukasyan, Appl. Phys. Lett. **101**(6), 063119 (2012).
[28]A. S. Rogachev, S. G. Vadchenko, F. Baras, O. Politano, S. Rouvimov, N. V. Sachkova, and A. S. Mukasyan, Acta Mater. **66**, 86 (2014).
[29]R. Armstrong, Metall. Trans. A **23**, 2339 (1992).
[30]I. E. Gunduz, K. Fadenberger, M. Kokonou, C. Rebholz, and C. C. Doumanidis, J. Appl. Phys. **105**, 074903 (2009).
[31]L. Alawieh, O. M. Knio, and T. P. Weihs, J. Appl. Phys. **110**, 013509 (2011).
[32]M. Salloum and O. M. Knio, Combust. Flame **157**, 1154 (2010).
[33]L. Alawieh, T. P. Weihs, and O. M. Knio, Combust. Flame **160**, 1857 (2013).
[34]C. Wagner, Acta Metall. Mater. **17**, 99 (1969).
[35]S. P. Garg, G. B. Kale, R. V. Patil, and T. Kundu, Intermetallics **7**, 901 (1999).
[36]A. Paul, A. A. Kodentsov, and F. J. J. van Loo, J. Alloys Compd. **403**, 147 (2005).
[37]R. D. Skeel and M. Berzins, SIAM J. Sci. Stat. Comput. **11**, 1 (1990).
[38]P. Zhu, J. C. M. Li, and C. T. Liu, Mater. Sci. Eng. A **357**, 248 (2003).
[39]O. Kubaschewski, C. B. Alcock, and P. J. Spencer, *Materials Thermochemistry*, 6th ed. (Pergamon Press, New York, 1993).
[40]V. I. Itin, G. A. Pribytkov, A. N. Tabachenko, and S. S. Borisov, Sov. Phys. J. **22**(4), 348 (1979).